NANO LETTERS

Letter

pubs.acs.org/NanoLett

Fluid and Highly Curved Model Membranes on Vertical Nanowire Arrays

Aleksandra P. Dabkowska,[†,‡] Cassandra S. Niman,[‡,§,$] Gaëlle Piret,[‡,§,⊗,$] Henrik Persson,[‡,§] Hanna P. Wacklin,[∥,⊥] Heiner Linke,[‡,§] Christelle N. Prinz,*[,‡,§,#] and Tommy Nylander*[,†,‡]

[†]Division of Physical Chemistry, Department of Chemistry, Lund University, P.O. Box 124, SE-22100 Lund, Sweden

[‡]The Nanometer Structure Consortium (nmC@LU), Lund University, P.O. Box 118, SE-22100 Lund, Sweden

[§]Division of Solid State Physics, Lund University, P.O. Box 118, SE-22100 Lund, Sweden

[∥]European Spallation Source ESS AB, P.O. Box 176, SE-221 00 Lund, Sweden

[⊥]Department of Chemistry, University of Copenhagen, Universitetsparken 5, 2100 Copenhagen, Denmark

[#]Neuronano Research Center, Lund University, SE-22184 Lund, Sweden

Supporting Information

ABSTRACT: Sensing and manipulating living cells using vertical nanowire devices requires a complete understanding of cell behavior on these substrates. Changes in cell function and phenotype are often triggered by events taking place at the plasma membrane, the properties of which are influenced by local curvature. The nanowire topography can therefore be expected to greatly affect the cell membrane, emphasizing the importance of studying membranes on vertical nanowire arrays. Here, we used supported phospholipid bilayers as a model for biomembranes. We demonstrate the formation of fluid supported bilayers on vertical nanowire forests using self-assembly from vesicles in solution. The bilayers were found to follow the contours of the nanowires to form continuous and locally highly curved model membranes. Distinct from standard flat supported lipid bilayers, the high aspect ratio of the nanowires results in a large bilayer surface available for the immobilization and study of biomolecules. We used these bilayers to bind a membrane-anchored protein as well as tethered vesicles on the nanowire substrate. The nanowire-bilayer platform shown here can be expanded from fundamental studies of lipid membranes on controlled curvature substrates to the development of innovative membrane-based nanosensors.

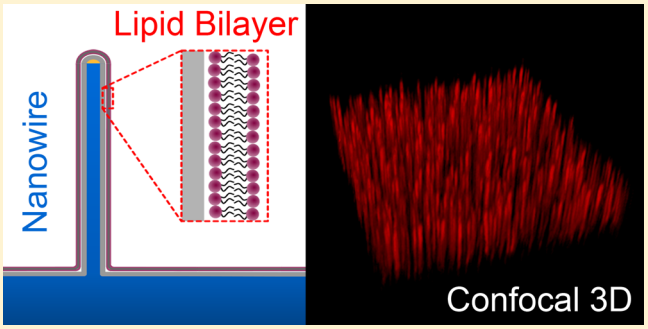

KEYWORDS: *Nanowires, lipid bilayer, membrane curvature, protein−lipid interaction, nanotopography, nanostructure*

Vertical nanowire (NW) arrays are increasingly finding their way into biotechnological applications, emerging as new nanometer-sized tools to probe and manipulate living cells. Nanowires have been used as waveguides for directed imaging[1] or sensing,[2] as probes of cellular signals[3−6] and forces,[7] as neuronal growth promoters[8−11] as well as vectors for intracellular delivery.[12−16] The effects of nanowires on cells are manifold. Recent studies have reported that cell migration is affected by the presence of vertical nanowires on the substrate.[17,18] Impeded and abnormal cell division has been reported for fibroblasts cultured on nanowire substrates.[17] However, the mechanisms that control the cell behavior observed on nanowires are not understood and there is limited knowledge about the nature of the contact that the cell makes with the nanowires.[19−21]

Of particular interest is the contact that occurs at the plasma membrane surface, as this interface is the first point of interaction with the cell. While some recent efforts have been made to discern whether the nanowires penetrate the plasma membrane of the cell,[13,17,20−23] a complete understanding of the interaction between nanowires and biological membranes is lacking. Membrane curvature, defined by its lipid/protein composition has been shown to influence membrane permeability and plays a crucial role in many cell functions,[24−26] such as mitosis. An exciting possibility is therefore to use supported lipid bilayers to probe the interaction between lipid membranes and nanowires presenting a well-defined surface curvature.

Supported lipid bilayers act not only as simple mimics of the cellular membrane's barrier function but also as a fluid lipid matrix that is capable of harboring functional membrane proteins, of which many are the target for the active compounds in modern medicine. The ability to use bilayers to couple membrane-bound molecules of interest to the nanowire surface opens up new possibilities for sensing of

Received: March 11, 2014
Revised: June 3, 2014
Published: June 27, 2014

   dx.doi.org/10.1021/nl500926y | *Nano Lett.* 2014, 14, 4286−4292

membrane processes and properties. These include, for example, the mechanical properties of the membrane itself as well as the detection of molecular binding to proteins or protein assemblies embedded or supported by the membrane.

Here, we show that supported lipid bilayers can be formed via vesicle fusion onto vertical nanowire forests. The dimensions of the nanowires were designed in such a way that the supported membranes on individual nanowires can be monitored in situ using fluorescence confocal microscopy. Diffusion coefficients extracted from fluorescence recovery after photobleaching (FRAP) experiments were used to verify the integrity of the supported bilayers and to understand how the topography of the underlying surface affects the conformation of the supported membrane. The nanowire-supported bilayer was used as a hybrid system to measure membrane-bound protein behavior as well as to tether vesicles to the nanowire surface.

We fabricated surfaces with vertical gallium phosphide (GaP) nanowires of varying nanowire spacing, length and diameter (see Supporting Information for detailed experimental protocol) to explore the full potential of the nanowire-forest-supported bilayers. GaP nanowires were selected as they can be produced to be uniform in their dimensions and to stand perfectly vertically on the surface with a highly controlled geometry using metal organic vapor phase epitaxy.[8,27] Scanning electron microscopy (SEM) images were used to measure the diameter, length, and density of the vertical nanowires on each sample (Figure 1a). A table with the sample dimensions is

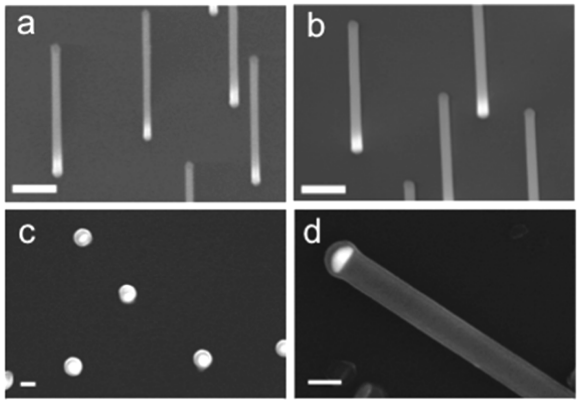

Figure 1. Scanning electron micrographs of vertical GaP nanowire forests, (a) before and (b) after deposition of SiO_x on the substrate. Stage tilt 20°, scale bars 500 nm. (c) Top view of vertical SiO_x-coated nanowire forest. Scale bar 100 nm. (d) Close-up of a single nanowire deposited on the surface displaying the gold nanoparticle used to seed nanowire epitaxial growth and SiO_x coating. Scale bar, 100 nm.

included in the Supporting Information (Table S1). In order to make the nanowires more compatible with bilayer formation and more amenable to surface modification,[28] a 20 nm thin layer of silicon oxide (SiO_x) was sputtered onto the surfaces. This resulted in a 7 nm SiO_x coating on the sides of the nanowires (Figure 1b–d). To confirm the uniformity of the oxide layer and verify that the shadowing effect had not prevented SiO_x from coating the entire nanowire walls, nanowires from a sample with high nanowire density (9 NW μm^{-2}) were transferred to a silicon wafer. The GaP core was selectively removed by immersing the sample in aqua regia.[12,29] SEM imaging revealed the remaining shell of SiO_x on the substrate, indicating that the sputter coating was able to cover the entire nanowire surface on even the densest sample (Figure S1 in the Supporting Information).

We formed fluorescently labeled phospholipid bilayers (20 mol % DOPE in DOPC with 0.5 mol % Rhod-PE) on GaP nanowire forests via in situ vesicle deposition and fusion (see the Supporting Information for the detailed experimental protocol). Before vesicle fusion we observed no fluorescence signal and after vesicle fusion, each nanowire appears as a dot, if viewed from the top (Figure 2a, inset). Visualization in the *z*-

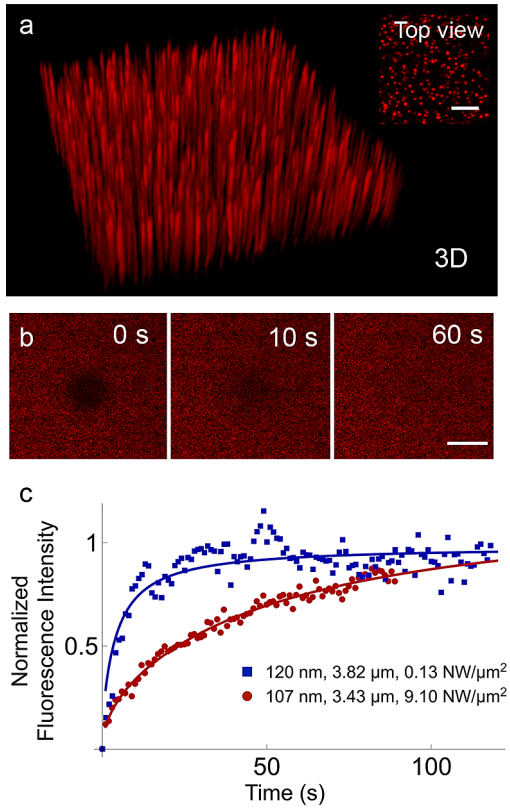

Figure 2. (a) 3D reconstruction of a confocal fluorescence z-stack of images of lipid bilayer on 6.8 μm long nanowires of 110 nm diameter at a density of 1.0 NW μm^{-2} (tilted surface area of 41 μm × 41 μm). The inset shows a top view of the fluorescence microscopy image of the nanowire forest, where each dot corresponds to a single nanowire. Scale bar 5 μm. (b) Images of fluorescence recovery of a lipid bilayer (20 mol % DOPE in DOPC with 0.5 mol % Rhod-PE) on a nanowire forest (5.2 NW μm^{-2}, a diameter of 100 nm, and a length of 2.8 μm). Images were taken directly after (0 s) bleaching a circular spot (diameter of 10 μm) and after recovery for 10 and 60 s. Scale bar 10 μm. (c) Typical normalized curves of fluorescence recovery (symbols) over time for nanowire arrays with different nanowire densities. The solid lines show the curve fits to the function describing the fluorescence recovery versus time (eq S1), as described in the Supporting Information.

direction by confocal microscopy shows that the lipid bilayer coats the entire length of the nanowires (Figure 2a). We confirmed the continuity and fluidity of the bilayers by performing FRAP experiments where we bleached a circular region of the fluorescent bilayer deposited on each nanowire forest and imaged as fluorescence recovered via lateral diffusion of fluorescent lipids within the bilayer (Figure 2b). Fluorescence recovery was observed for all nanowire substrate geometries indicating that fluorescent lipids can diffuse freely on vertical nanowire arrays (Figure 2c). The fraction of lipids

dx.doi.org/10.1021/nl500926y | *Nano Lett.* 2014, 14, 4286–4292

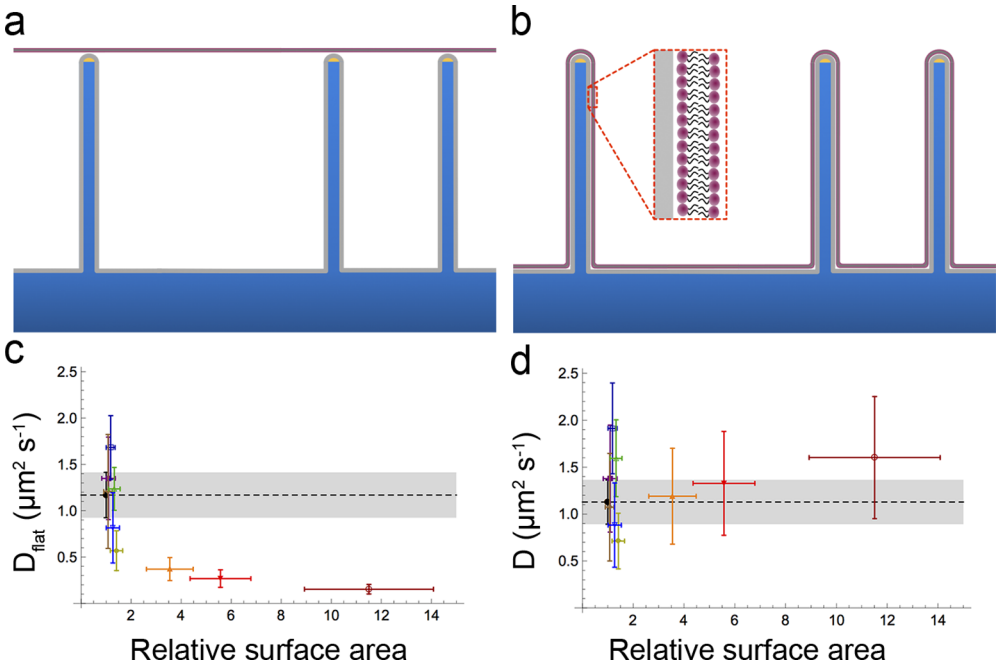

Figure 3. Schematic cross section through a nanowire forest where the bilayer (a) spans across the top of the nanowires or (b) follows the contours of the nanowire forest. Scaled diffusion coefficients for the two scenarios, D_{flat} for the bilayer spanning on top of the nanowires (c) or D for the bilayer following the contours of the nanowires (d). The dashed line shows the expected diffusion coefficient extrapolated from the measured diffusion coefficient on a flat surface, with the measurement error shown as a gray area around the dashed line. The y-axis error bars are the standard deviation of the mean diffusion coefficient while error bars on the x-axis show the standard error on the surface area, as determined from SEM measurements. Color coding as outlined in Table S1 in the Supporting Information.

that are mobile on the surface and contribute to the recovery of the fluorescent signal corresponds to the ratio of the total intensity after recovery over the total intensity before bleaching (Figure 2c). The mobile fraction was determined to be 0.86 ± 0.12 (mean value for all samples measured ± SD), indicating that most fluorescent lipids are contained within bilayers that are both fluid and continuous.

Figure 3 depicts the possible topographies of a bilayer giving the minimal (a) and maximal (b) bilayer surface area. In the first case, the bilayer spans across the nanowire tips, forming a continuous layer over the nanowire forest and resulting in a "bed of nails" topography (Figure 3a). In the other case, the bilayer follows the contours of the nanowires on the surface (Figure 3b). Several observations together provide strong evidence that in our case, the bilayer follows the contours of the nanowires (maximal bilayer surface area model, Figure 3b): (i) we captured z-stack images of the bilayers using confocal microscopy and observed fluorescence along the length of the nanowires (Figure 2a; Figure S2 in the Supporting Information), indicating that bilayers formed on the side facets of the nanowires; (ii) the apparent recovery of fluorescence after photobleaching was slower for surfaces with higher densities of nanowires (Figure 2c); (iii) similarly, we observed that when two surfaces with the same nanowire densities were compared, the apparent diffusivity was lower on surfaces containing longer nanowires (Figure S3a in the Supporting Information). These results suggest that the apparent recovery time depends on the substrate surface area alone (and thus the distance that the molecules must traverse).

In order to analyze quantitatively the effect of substrate topography, we used the apparent diffusivity to model the bilayer topography and properties on the nanoarchitecture of the surface. We calculated the effective diffusivity of lipids when taking into account the bilayer effective surface area for all samples listed in Table S1 in the Supporting Information and for each geometry depicted in Figure 3a,b. The diffusivity was scaled according to the calculated increase in bilayer surface area for each of the two topographies (Figure 3c,d).

The relationship between the apparent diffusion coefficient and an increase in bilayer-surface area caused by nanostructures on a surface was previously described by Jönsson et al. for bilayers that conform to the topography of nonperiodic, cylindrical, submicron wells.[30] In the case of bilayers on the nanowire arrays, the calculated diffusion coefficient, D, takes into account the surface area of the nanowires as given by

$$D = D_{flat}(1 + \pi dl\rho) \quad (1)$$

where d and l are the diameter and length of the nanowires, respectively, and ρ is the density of nanowires on the surface. D_{flat} is the diffusion coefficient calculated for a flat region in a bleach spot of radius w. Because of the laser bleaching beam's uniform circular profile, we used the Soumpasis method[31] for fitting the normalized intensity in the bleached spot (details in the Supporting Information), resulting in a characteristic diffusion time, τ_D, where

$$D_{flat} = \frac{w^2}{4\tau_D} \quad (2)$$

The dashed line in Figure 3c,d shows the calculated model for the diffusion coefficient that would be expected for lipids in the bilayer, assuming that the lipid diffusivity on the nanowires is similar to that on the flat regions. One would expect this diffusion constant to be independent of surface area. While there is a large discrepancy between the expected diffusion constant and the experimental data analyzed using the minimal bilayer surface area model (bed of nails, Figure 3a,c), the model

dx.doi.org/10.1021/nl500926y | Nano Lett. 2014, 14, 4286−4292

that assumes the bilayer follows the contours of the nanowires (maximum bilayer surface area) fits the data well (Figure 3d). This analysis supports the observations from the confocal z-stack imaging and corroborates the hypothesis that the topography of the bilayers follows that of the nanowires. We also find the same fluorescence recovery for bilayers deposited on samples where the SiO_x layer was formed via atomic layer deposition (ALD) instead of sputtering. Our results are consistent with the findings of a previous study investigating the effects of substrate curvature on supported bilayers, where bilayers were found to conform to the support, albeit at lower curvatures (semispheres with diameters down to 110 nm).[32]

The fact that the lipid bilayer follows the contours of the nanowires (Figure 3b) instead of spanning across the nanowire tips (Figure 3a) can be explained by the nanowire forest morphology as well as the lipid packing constraints at curved interfaces.[33] For the lipids used in this study, DOPC and DOPE, the values of spontaneous interfacial curvature corresponding to the ideal lipid packing are -0.1 nm^{-1} and -0.48 nm^{-1}, respectively.[34] Here the negative sign indicates that the lipid layer tends to curve toward the surrounding water phase. For the 80:20 DOPC−DOPE lipid mixture, the curvature is expected to be -0.176 nm^{-1}, corresponding to a 5.7 nm radius. This means that bilayer is able to curve down to this radius without imposing stress.[37] As long as the radius of the supporting structure is larger than this value, it will always be favorable to form a supported bilayer.

For a given nanowire substrate, the most curved interface has the radius equal to that of the individual nanowires. The nanowires used in this study had radii of 35−60 nm after sputter coating with SiO_x (Table S1 in the Supporting Information), which is considerably larger than the radius corresponding to the spontaneous curvature of the DOPC-DOPE bilayer. Therefore, we can expect the bilayer to always follow the contours of the nanowires, provided that it is possible for the vesicles to access the surface. This was the case even for substrates with the highest nanowire density ($\approx$10 NW μm^{-2}). Indeed, at this density, the average distance between nanowires is about 300 nm, which is larger than the diameter of the sonicated vesicles. Conversely, for a vesicle to fit between nanowires at higher density than about 80 NW μm^{-2}, the curvature imposed on the bilayer would exceed the spontaneous curvature for the used lipid mixture. We can therefore conclude that the formation of a bilayer that follows the nanowire surfaces results from the relatively large radii of the nanowires and the distances between them.

The effect of nanowire curvature was observed by Fu et al.[35] who used lipid-coated BIT-FET nanotubes with 5−7.5 nm inner radius to record intracellular signals. The lipid used, dimyristoylphosphatidylcholine (DMPC), has a slightly positive spontaneous curvature ($+0.1$ nm^{-1}),[36] translating to a radius of 10 nm, which is slightly larger than the inner radius of the nanotube. This would suggest little or no lipid bilayer deposition. However, the expanding inner radius toward the lower end of the nanotube (up to 80 nm) explains why partial lipid coverage was observed in some cases. This can occur at least to some extent if the lipid−substrate attractive interaction is very strong.

The formation of bilayers that follow the contours of the nanostructured surfaces with exceptionally high aspect ratio studied here provides many advantages for sensing applications. For instance, the lipid−nanowire hybrids offer the possibility to vary the physical properties of the lipid bilayer itself, as the highly controlled surface topographies of nanowire forests can be used to define the curvature of fluid supported bilayers by varying the diameter of the nanowires. These curved regions can be uniquely valuable in systematic studies of the influence of curvature on biomolecules at lipid membranes. Further, while it has been shown that lipid bilayers form on silicon nanowire field effect transistors,[38,39] as well as on a single silicon nanowire laid horizontally[40] and nanowires dispersed in solution,[41] the possibility to use arrays of vertical nanowires−bilayer hybrid structures opens up the capabilities to study interactions at the membrane interface using a range of surface sensitive techniques. Unlike dispersed nanowires, the nanowires here are vertically aligned and attached to a surface, a feature that will potentially enable us to localize and track interactions taking place at any individual nanowire.

In this study, we also probed the feasibility of the nanowire−bilayer hybrids to serve as a suitable system for studying membrane-associated proteins. We anchored the streptavidin protein to the fluid matrix of the membrane via specific binding to a biotinylated lipid. We first formed a bilayer containing both the fluorescently labeled lipids (Rhod-PE, red) as well the biotinylated anchoring lipids onto nanowires and used FRAP measurements to verify that the bilayer was fluid and continuous. The molar fraction of biotinylated lipids was held constant at 0.005, while the concentration of fluorescence-labeled streptavidin (FITC, green) was gradually increased. For each concentration of streptavidin, the bilayer−nanowire surfaces were incubated for 1 h with the protein and subsequently rinsed with buffer and imaged using fluorescence microscopy (see the Supporting Information for detailed experimental protocol). The sequential increase of the fluorescently labeled protein concentration resulted in increasing green fluorescence intensity (Figure 4a,b), confirming the binding of streptavidin to the bilayer. Importantly, even after streptavidin was anchored in the bilayer, the nanowire-supported bilayer retained its fluidity, as shown by the red fluorescence recovery obtained in FRAP experiments (Figure 4c). Bleaching the fluorescent label of the protein resulted in slower recovery of streptavidin compared to the recovery of the lipid probes (Figure 4c). This finding is consistent with the much slower diffusion of proteins compared to lipids due to their larger size as well as with the fact that each streptavidin can be anchored to up to four biotinylated lipids. Experiments of protein binding were also performed using bilayers without the fluorescent lipids and yielded similar results. When normalized to surface area, the FITC-streptavidin fluorescence curves for the three substrates do not overlap (Figure S4 in the Supporting Information), suggesting that the nanowire curvature has an effect on the local protein concentration.

Note that incubation of streptavidin with nanowire-supported bilayers not containing the anchoring lipid (biotinylayed PE) resulted in no detectable binding onto the nanowire forests (Figure S6 in the Supporting Information). This shows that the bilayer passivates the nanowire substrate with respect to nonspecific protein adsorption. The use of lipid bilayers as a robust and self-assembling passivation layer has been shown to perform well in nanodevices[42] and would also do so for the increasing number of nanowire technology-based applications.

One further benefit of the nanowire forest is that the nanostructures produce an enormous increase in the surface area. In terms of membrane-associated proteins, this results in a much higher concentration of proteins on the surface, an

dx.doi.org/10.1021/nl500926y | Nano Lett. 2014, 14, 4286−4292

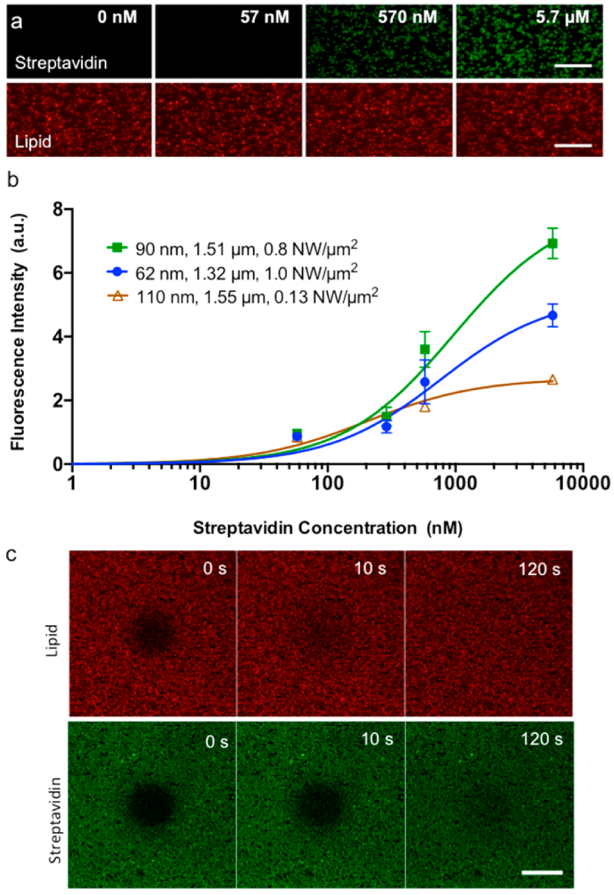

Figure 4. (a) Fluorescence micrographs after addition of different concentrations of streptavidin (FITC-labeled) to biotinylated lipids in bilayers formed on SiO_x-coated GaP nanowire forests (density 0.65 NW μm^{-2}, length 1.51 μm, diameter 90 nm). The fluorescence of the lipids and the FITC-labeled streptavidin are shown. (b) Fluorescence intensity as a function of protein concentration incubated with nanowire forests of different topography (as shown in the legend). Line to guide the eye. (c) FRAP measurements of lipids and lipid-tethered FITC-streptavidin (incubation with 2.3 μM FITC streptavidin) in bilayers on nanowire forests of density 7.3 NW μm^{-2}, length 1.1 μm, and diameter 100 nm. Images were taken directly after (0 s) bleaching a circular spot (diameter of 10 μm) and after recovery for 10 and 120 s. Scale bar 10 μm.

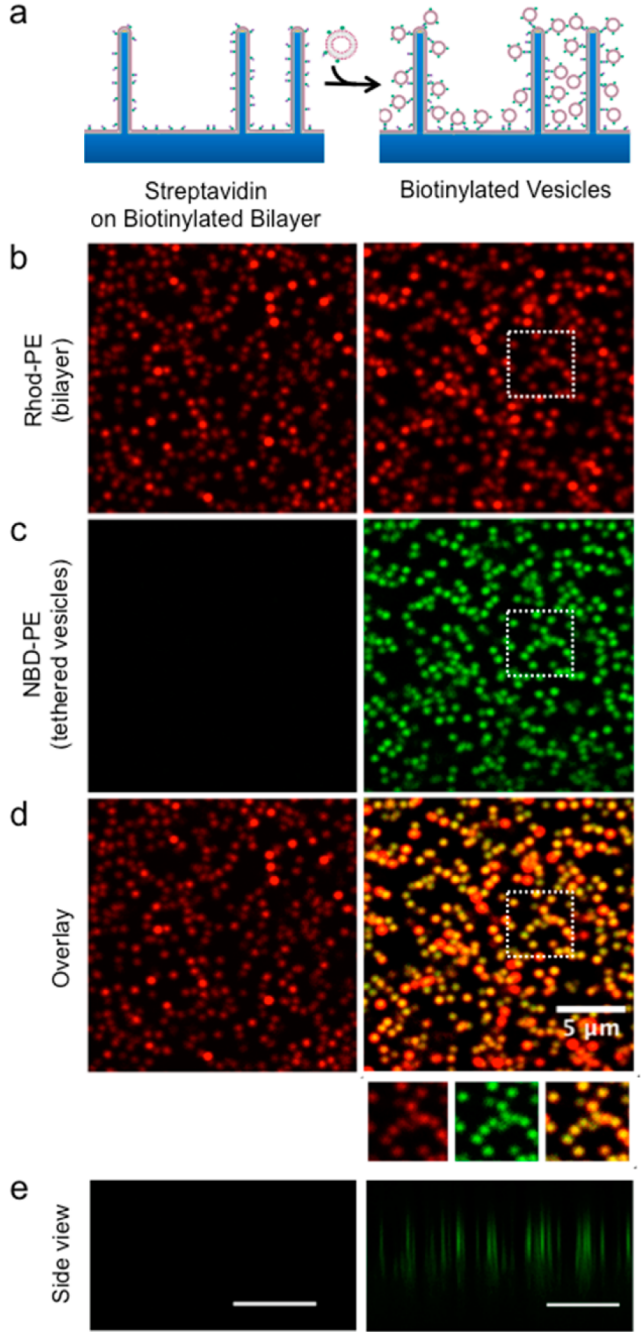

Figure 5. (a) Schematic representation of addition of biotinylated vesicles (NBD labeled) to streptavidin-coated bilayers on vertical nanowire arrays. Micrographs showing a top-view of (b) the bilayer (Rhod-PE) fluorescence, (c) the vesicle fluorescence (NBD-PE) and (d) the overlay of the two channels. For panels b–d, the dot-like features in the image are a top view of the nanowires, with each dot corresponding to one nanowire. The squares in panels b–d are to guide the eye to the distribution of the nanowires. A close up view of the squares is shown below panel d. The side view of the vesicle NBD fluorescence is shown in panel e. Scale bars, 10 μm.

important feature that has been previously exploited for nanowire-based sensing applications.[43,44]

Finally, we tested whether the hybrid bilayer-nanowire platform could also provide a route to more complex surface assemblies, such as surface tethered vesicles (see Figure 5a). Tethered vesicles provide an analytical tool to study membrane processes, such as membrane fusion[45] and single enzyme kinetics[46] using high-throughput surface sensitive techniques, as reviewed in ref 47. Fluid supported bilayers containing biotinylated lipids and labeled with Rhod-PE were first prepared by vesicle fusion, as described above. Unlabeled streptavidin was then injected in the flow cell, allowed to react with the biotinylated lipids and the excess was rinsed off. Subsequently, vesicles containing biotinylated lipids with a green probe (NBD-PE) were added on top of the streptavidin-coated bilayer. After rinsing, the fluorescent vesicles were observed to remain attached to the surface (Figure 5b–e). Bearing in mind the size of the vesicles (diameters less than 100 nm), it is not possible to resolve individual vesicles. Instead, what we observe in Figure 5c is the green fluorescent intensity of more than one vesicle tethered to each of the nanowires. The vesicles are localized in the vicinity of the nanowires as the green fluorescence (labeled with NBD-lipids) from the tethered vesicles is observed in the same regions as that of the red bilayer fluorescence. While the tethered vesicles were found not to

dx.doi.org/10.1021/nl500926y | Nano Lett. 2014, 14, 4286–4292

diffuse (no recovery after photobleaching) as expected from their large dimensions, the underlying supported bilayer was found to recover showing that it remained fluid and continuous.

In conclusion, we have demonstrated that it is possible for lipid bilayers, serving as simple models of cellular membranes, to self-assemble onto vertically aligned nanowires via facile, in situ fusion of lipid vesicles. The bilayers follow the nanowire forest topography over millimeter-sized areas. We have shown that it is possible to monitor the binding of lipid-bound peripheral membrane proteins to the nanowire-supported bilayers and that it is possible to tether vesicles to the bilayer. Nanowire-supported bilayers therefore offer the possibility to tune the chemical composition of the surface by varying the bilayer composition and thereby enable the detection of specific membrane-associated molecular events. Moreover, the hybrid bilayer-nanowire system can also provide an increased sensitivity due to a much larger membrane area that could be used for bionanoelectronics. Given the diversity of membrane morphologies involved in biologically relevant interactions, it is interesting to examine membrane systems that have an imposed curved surface topography. In the nanowire-supported bilayers presented here, the precisely controlled curvature enables studies of the influence of curvature on biomolecules at lipid membranes, which may shed light on cell function and behavior when interfaced with nanowire arrays.

■ ASSOCIATED CONTENT

Ⓢ Supporting Information

Experimental section with detailed descriptions of materials and methods used in the study, Table S1 summarizing the dimensions of the nanowire forest used in this study, Figure S1 showing SEM images of the SiO_x coating on GaP nanowires, Figure S2 showing confocal fluorescence *z*-axis images of different nanowire forest geometries, Figure S3 showing the apparent lipid diffusion as a function of nanowire length, Figure S4 showing the fluorescence intensity scaled by the surface area, Figure S5 showing the characterization of streptavidin anchoring to lipid bilayers and Figure S6 showing fluorescence recovery of bilayers on glass. This material is available free of charge via the Internet at http://pubs.acs.org.

■ AUTHOR INFORMATION

Corresponding Authors

*E-mail: christelle.prinz@ftf.lth.se.
*E-mail: tommy.nylander@fkem1.lu.se.

Present Address

[⊗]G.P.: INSERM, Clinatec, Minatec Campus, 17 Rue des Martyrs, 38054 Grenoble Cedex 09, France.

Author Contributions

[$]C.S.N. and G.P. contributed equally to this work.

Notes

The authors declare no competing financial interest.

■ ACKNOWLEDGMENTS

This work was supported by nmC@LU, the Swedish Research Council (VR) via the Linnaeus Center of Excellence "Organizing molecular matter" and Grant 621-2010-4527, as well as by the Carl Trygger Foundation. The QCM-D equipment and the confocal microscope were purchased with funding obtained from the Knut and Alice Wallenberg Foundation. We thank Karl Adolfsson for assistance with nanowire growth, Debby Chang, Peter Jönsson, and Nicklas Anttu for helpful discussions, Anders Kvennefors for help with ALD and SEM, as well as Christopher Hirst for technical support. All nanowire substrates were fabricated at Lund Nano Lab.

■ ABBREVIATIONS

NW, nanowire; FRAP, fluorescence recovery after photobleaching; Rhod-PE, 1,2-dioleoyl-*sn*-glycero-3-phosphoethanolamine-*N*-(lissamine rhodamine B sulfonyl) (ammonium salt); FITC, fluorescein-isothiocyanate; SEM, scanning electron microscopy

■ REFERENCES

(1) Xie, C.; Hanson, L.; Cui, Y.; Cui, B. Vertical Nanopillars for Highly Localized Fluorescence Imaging. *Proc. Natl. Acad. Sci. U.S.A.* **2011**, *8*, 3894−3899.

(2) ten Siethoff, L.; Lard, M.; Generosi, J.; Andersson, H. S.; Linke, H.; Månsson, A. Molecular Motor Propelled Filaments Reveal Light-Guiding in Nanowire Arrays for Enhanced Biosensing. *Nano Lett.* **2014**, *14*, 737−742.

(3) Robinson, J. T.; Jorgolli, M.; Shalek, A. K.; Yoon, M.-H.; Gertner, R. S.; Park, H. Vertical Nanowire Electrode Arrays as a Scalable Platform for Intracellular Interfacing to Neuronal Circuits. *Nat. Nanotechnol.* **2012**, *7*, 180−184.

(4) Duan, X. J.; Gao, R. X.; Xie, P.; Cohen-Karni, T.; Qing, Q.; Choe, H. S.; Tian, B. Z.; Jiang, X. C.; Lieber, C. M. *Nat. Nanotechnol.* **2012**, *7*, 174−179.

(5) Xie, C.; Lin, Z. L.; Hanson, L.; Cui, Y.; Cui, B. X. *Nat. Nanotechnol.* **2012**, *7*, 185−190.

(6) Suyatin, D. B.; Wallman, L.; Thelin, J.; Prinz, C. N.; Jorntell, H.; Samuelson, L.; Montelius, L.; Schouenborg, J. *PLoS One* **2013**, *8*, e566673.

(7) Hällström, W.; Lexholm, M.; Suyatin, D. B.; Hammarin, G.; Hessman, D.; Samuelson, L.; Montelius, L.; Kanje, M.; Prinz, C. N. Fifteen-Piconewton Force Detection from Neural Growth Cones Using Nanowire Arrays. *Nano Lett.* **2010**, *10*, 782−787.

(8) Hällström, W.; Mårtensson, T.; Prinz, C.; Gustavsson, P.; Montelius, L.; Samuelson, L.; Kanje, M. Gallium Phosphide Nanowires as a Substrate for Cultured Neurons. *Nano Lett.* **2007**, *7*, 2960−2965.

(9) Hällström, W.; Prinz, C. N.; Suyatin, D.; Samuelson, L.; Montelius, L.; Kanje, M. Rectifying and Sorting of Regenerating Axons by Free-Standing Nanowire Patterns: a Highway for Nerve Fibers. *Langmuir* **2009**, *25*, 4343−4346.

(10) Piret, G.; Perez, M.-T.; Prinz, C. N. Neurite Outgrowth and Synaptophysin Expression of Postnatal CNS Neurons on GaP Nanowire Arrays in Long-Term Retinal Cell Culture. *Biomaterials* **2013**, *34*, 875−887.

(11) Prinz, C.; Hällström, W.; Mårtensson, T.; Samuelson, L.; Montelius, L.; Kanje, M. Axonal Guidance on Patterned Free-Standing Nanowire Surfaces. *Nanotechnology* **2008**, *19*, 345101.

(12) Persson, H.; Beech, J. P.; Samuelson, L.; Oredsson, S.; Prinz, C. N.; Tegenfeldt, J. O. Vertical Oxide Nanotubes Connected by Subsurface Microchannels. *Nano Res.* **2012**, *5*, 190−198.

(13) Mumm, F.; Beckwith, K. M.; Bonde, S.; Martinez, K. L.; Sikorski, P. A Transparent Nanowire-Based Cell Impalement Device Suitable for Detailed Cell-Nanowire Interaction Studies. *Small* **2013**, *9*, 263−272.

(14) Sköld, N.; Hällström, W.; Persson, H.; Montelius, L.; Kanje, M.; Samuelson, L.; Prinz, C. N.; Tegenfeldt, J. O. Nanofluidics in Hollow Nanowires. *Nanotechnology* **2010**, *21*, 155301.

(15) VanDersarl, J. J.; Xu, A. M.; Melosh, N. Nanostraws for Direct Fluidic Intracellular Access. *Nano Lett.* **2012**, *12*, 3881−3886.

(16) Shalek, A. K.; Robinson, J. T.; Karp, E. S.; Lee, J. S.; Ahn, D.-R.; Yoon, M.-H.; Sutton, A.; Jorgolli, M.; Gertner, R. S.; Gujral, T. S.; et al. Vertical Silicon Nanowires as a Universal Platform for Delivering Biomolecules into Living Cells. *Proc. Natl. Acad. Sci. U.S.A.* **2010**, *107*, 1870−1875.

(17) Persson, H.; Køber, C.; Mølhave, K.; Samuelson, L.; Tegenfeldt, J. O.; Oredsson, S.; Prinz, C. N. Fibroblasts Cultured on Nanowires Exhibit Low Motility, Impaired Cell Division, and DNA Damage. *Small* **2013**, *9*, 4006−4016.
(18) Xie, C.; Hanson, L.; Xie, W. J.; Lin, Z. L.; Cui, B. X.; Cui, Y. Noninvasive Neuron Pinning with Nanopillar Arrays. *Nano Lett.* **2010**, *10*, 4020−4024.
(19) Adolfsson, K.; Persson, H.; Wallentin, J.; Oredsson, S.; Samuelson, L.; Tegenfeldt, J. O.; Borgström, M. T.; Prinz, C. N. Fluorescent Nanowire Heterostructures as a Versatile Tool for Biology Applications. *Nano Lett.* **2013**, *13*, 4728−4732.
(20) Hanson, L.; Lin, Z. C.; Xie, C.; Cui, Y.; Cui, B. X. Characterization of the Cell−Nanopillar Interface by Transmission Electron Microscopy. *Nano Lett.* **2012**, *12*, 5815−5820.
(21) Berthing, T.; Bonde, S.; Rostgaard, K. R.; Madsen, M. H.; Sorensen, C. B.; Nygard, J.; Martinez, K. L. Cell Membrane Conformation at Vertical Nanowire Array Interface Revealed by Fluorescence Imaging. *Nanotechnology* **2012**, *23*, 415102.
(22) Xie, X.; Xu, A. M.; Angle, M. R.; Tayebi, N.; Verma, P.; Melosh, N. a Mechanical Model of Vertical Nanowire Cell Penetration. *Nano Lett.* **2013**, *13*, 6002−6008.
(23) Yi, X.; Shi, X.; Gao, H. A Universal Law for Cell Uptake of One-Dimensional Nanomaterials. *Nano Lett.* **2014**, *14*, 1049−1055.
(24) Domart, M.-C.; Hobday, T. M. C.; Peddie, C. J.; Chung, G. H. C.; Wang, A.; Yeh, K.; Jethwa, N.; Zhang, Q. F.; Wakelam, M. J. O.; Woscholski, R.; et al.. Acute Manipulation of Diacylglycerol Reveals Roles in Nuclear Envelope Assembly & Endoplasmic Reticulum Morphology. *PLoS One* **2012**, 7e51150.
(25) Parthasarathy, R.; Yu, C.; Groves, J. T. Curvature-Modulated Phase Separation in Lipid Bilayer Membranes. *Langmuir* **2006**, *22*, 5095−5099.
(26) Tabaei, S. R.; Rabe, M.; Zhdanov, V. P.; Cho, N.-J. J.; Höök, F. Single Vesicle Analysis Reveals Nanoscale Membrane Curvature Selective Pore Formation in Lipid Membranes by an Antiviral α-Helical Peptide. *Nano Lett.* **2012**, *12*, 5719−5725.
(27) Suyatin, D. B.; Hällström, W.; Samuelson, L.; Montelius, L.; Prinz, C. N.; Kanje, M. Gallium Phosphide Nanowire Arrays and Their Possible Application in Cellular Force Investigations. *J. Vac. Sci. Technol., B: Microelectron. Nanometer Struct.* **2009**, *27*, 3092.
(28) Reimhult, E.; Kasemo, B.; Höök, F. Rupture Pathway of Phosphatidylcholine Liposomes on Silicon Dioxide. *Int. J. Mol. Sci.* **2009**, *10*, 1683−1696.
(29) Chang, K. L.; Lee, C. K.; Hsu, J. W.; Hsieh, H. F.; Shih, H. C. The Etching Behavior of n-GaP in Aqua Regia Solutions. *J. Appl. Electrochem.* **2005**, *35*, 77−84.
(30) Jönsson, P.; Jonsson, M. P.; Höök, F. Sealing of Submicrometer Wells by a Shear-Driven Lipid Bilayer. *Nano Lett.* **2010**, *10*, 1900−1906.
(31) Soumpasis, D. M. Theoretical Analysis of Fluorescence Photobleaching Recovery Experiments. *Biophys. J.* **1983**, *41*, 95−97.
(32) Sundh, M.; Svedhem, S.; Sutherland, D. S. Formation of Supported Lipid Bilayers at Surfaces with Controlled Curvatures: Influence of Lipid Charge. *J. Phys. Chem. B* **2011**, *115*, 7838−7848.
(33) Israelachvili, J. N.; Mitchell, D. J.; Ninham, B. W. Theory of Self-Assembly of Lipid Bilayers and Vesicles. *Biochim. Biophys. Acta* **1977**, *470*, 185−201.
(34) Hamai, C.; Yang, T.; Kataoka, S.; Cremer, P. S.; Musser, S. M. Effect of Average Phospholipid Curvature on Supported Bilayer Formation on Glass by Vesicle Fusion. *Biophys. J.* **2006**, *90*, 1241−1248.
(35) Fu, T.-M.; Duan, X.; Jiang, Z.; Dai, X.; Xie, P.; Cheng, Z.; Lieber, C. M. Sub-10 nm Intracellular Bioelectronic Probes from Nanowire-Nanotube Heterostructures. *Proc. Natl. Acad. Sci. U.S.A.* **2014**, *111*, 1259−1264.
(36) Orsi, M.; Michel, J.; Essex, J. W. Coarse-Grain Modelling of DMPC and DOPC Lipid Bilayers. *J. Phys.: Condens. Matter* **2010**, *22*, 155106.
(37) Helfrich, W. Elastic Properties of Lipid Bilayers: Theory and Possible Experiments. *Z. Naturforsch* **1973**, *28*, 693−703.
(38) Tian, B.; Cohen-Karni, T.; Qing, Q.; Duan, X.; Ping, X.; Lieber, C. M. Three-Dimensional, Flexible Nanoscale Field-Effect Transistors as Localized Bioprobes. *Science* **2010**, *329*, 830−834.
(39) Jiang, Z.; Qing, Q.; Xie, P.; Gao, R.; Lieber, C. M. Kinked p-n Junction Nanowire Probes for High Spatial Resolution Sensing and Intracellular Recording. *Nano Lett.* **2012**, *12*, 1711−1716.
(40) Huang, S.-C. J.; Artyukhin, A. B.; Martinez, J. A.; Sirbuly, D. J.; Wang, Y.; Ju, J.-W.; Stroeve, P.; Noy, A. Formation, Stability, and Mobility of One-Dimensional Lipid Bilayers on Polysilicon Nanowires. *Nano Lett.* **2007**, *7*, 3355−3359.
(41) Römhildt, L.; Gang, A.; Baraban, L.; Opitz, J.; Cuniberti, G. High Yield Formation of Lipid Bilayer Shells Around Silicon Nanowires in Aqueous Solution. *Nanotechnology* **2013**, *24*, 355601.
(42) Persson, F.; Fritzsche, J.; Mir, K. U.; Modesti, M.; Westerlund, F.; Tegenfeldt, J. O. Lipid-Based Passivation in Nanofluidics. *Nano Lett.* **2012**, *12*, 2260−2265.
(43) Rostgaard, K. R.; Frederiksen, R. S.; Liu, Y.-C. C.; Berthing, T.; Madsen, M. H.; Holm, J.; Nygård, J.; Martinez, K. L. Vertical Nanowire Arrays as a Versatile Platform for Protein Detection and Analysis. *Nanoscale* **2013**, *5*, 10226−10235.
(44) Krivitsky, V.; Hsiung, L.-C.; Lichtenstein, A.; Brudnik, B.; Kantaev, R.; Elnathan, R.; Pevzner, A.; Khatchtourints, A.; Patolsky, F. Si Nanowires Forest-Based on-Chip Biomolecular Filtering, Separation and Preconcentration Devices: Nanowires Do It All. *Nano Lett.* **2012**, *12*, 4748−4756.
(45) van Lengerich, B.; Rawle, R. J.; Bendix, P. M.; Boxer, S. G. Individual Vesicle Fusion Events Mediated by Lipid-Anchored DNA. *Biophys. J.* **2013**, *105*, 409−419.
(46) Tabaei, S. R.; Rabe, M.; Zetterberg, H.; Zhdanov, V. P.; Höök, F. Single Lipid Vesicle Assay for Characterizing Single-Enzyme Kinetics of Phospholipid Hydrolysis in a Complex Biological Fluid. *J. Am. Chem. Soc.* **2013**, *135*, 14151−14158.
(47) Christensen, S. M.; Stamou, D. G. Sensing-Applications of Surface-Based Single Vesicle Arrays. *Sensors* **2010**, *10*, 11352−11368.